Self-affine fractal distributions of the bulk density, elastic moduli, and seismic wave velocities of rock

Muhammad Sahimi and S. Ehsan Tajer
Department of Chemical Engineering, University of Southern California, Los Angeles, California 90089-1211, USA
(Received 1 December 2004; published 4 April 2005)

The scale dependence of the bulk density ρ and seismic wave velocities V_p and V_s and the possibility of the existence of long-range correlations in such properties in field-scale porous media (FSPM) are investigated. We analyze measured data for ρ, V_p, and V_s for nine FSPM, using the maximum entropy method and the wavelet decomposition technique. The analysis indicates the existence of long-range correlations in the data, characterized by self-affine fractal distributions that follow the statistics of the fractional Brownian motion. Therefore, the elastic moduli of the FSPM should also be fractally distributed and contain long-range correlations; our analysis confirms this. The implications of the results for modeling elastic moduli of porous rock, fracture propagation in FSPM, and the interpretation of seismic wave recordings of FSPM are discussed, and the possible deviations from the classical analysis of such phenomena are pointed out.

DOI: 10.1103/PhysRevE.71.046301 PACS number(s): 47.55.Mh, 47.53.+n, 91.60.Lj

I. INTRODUCTION

Natural porous media are highly heterogeneous at many length scales, ranging from pore to laboratory [1–3] and field scales [1,3]. In particular, in field-scale porous media (FSPM), such as oil and gas reservoirs and groundwater aquifers, the porosity, permeability, elastic moduli, bulk density, seismic wave velocities, and other properties are broadly distributed. Better understanding of the geology of FSPM, and in particular the distributions of their morphological, flow, and geophysical properties, is critical to the modeling of a wide variety of important processes in such formations, such as flow of fluids, nucleation and propagation of fracture, seismic wave propagation, and earthquakes.

To model the geology of FSPM, one must first analyze the existing data for their various properties. The data may be divided into two groups. (1) In one group are what are usually called the *direct* data, which include measured distributions of the porosity, permeability, elastic moduli, and bulk density. Such data provide direct information on the morphology of FSPM and their effective properties. (2) *Indirect* data, the most important of which are seismic recordings, are in the second group. They do not provide any information on the permeability distribution which is crucial to the flow of fluids in FSPM, but yield insight into the large-scale structure of FSPM, as well as the distribution of the porosity.

Field-scale porous media are usually stratified and contain a number of layers of different properties. Hewett [4] provided the first concrete evidence that the porosity logs in the direction perpendicular to the bedding may follow the statistics of a fractional Gaussian noise (FGN), while those parallel to the bedding follow a fractional Brownian motion (FBM). The semivariogram of a set of data is defined by

$$\gamma(r) = \frac{1}{2}\langle [p(r) - p(r+r')]^2 \rangle, \tag{1}$$

where $p(r)$ is the the datum measured at r and the averaging is over all the values of r. The semivariogram of a one-dimensional (1D) set of data that follow the statistics of an FGN is given by [5]

$$\gamma(r) = \gamma_0 s^{2H} - \frac{\gamma_1}{2s^2}[(r+s)^{2H} - 2r^{2H} + |r-s|^{2H}], \tag{2}$$

where s is a smoothing parameter, γ_0 and γ_1 are two constants, and H is the Hurst exponent. The spectral density of a 1D FGN—the Fourier transform of its covariance—is then given by

$$S(\omega) = \frac{1}{\pi}\gamma_0 H\Gamma(2H)\sin(\pi H)\frac{1}{\omega^{2H-1}}. \tag{3}$$

For frequencies $\omega \gg 1/s$ the spectral density of a FGN becomes negative (and unphysical). The corresponding spectral density of a 1D FBM is given by

$$S(\omega) = \frac{\gamma_0 H}{\Gamma(1-2H)\cos(\pi H)}\frac{1}{\omega^{2H+1}}. \tag{4}$$

Note that $H > 0.5$ (< 0.5) indicates positive (negative) correlations in the data, with the extent of the correlations being the thickness of the zone in which the data are collected, while $H = 0.5$ implies that successive increments in the data are random and follow a Brownian motion.

Extensive studies [6–11] have provided strong evidence that the porosity logs of FSPM often follow the statistics of a FGN or FBM and that, in most cases (to within a few percent), $H \simeq 0.85$. Similarly, measurements on outcrop surfaces provided evidence [12–14] that, in many cases, the permeability distributions follow Eqs. (3) and (4). For example, the analysis of Goggin *et al.* [12] on sandstone outcrop data indicated that the logarithm of the permeabilities along the lateral trace follow the FGN statistics with $H \simeq 0.85$, while Neuman [15] presented strong evidence that the permeability distributions of many aquifers follow the statistics of a FBM with $H < 0.5$. Others [11,16,17] provided evidence that, at least in some cases, the porosities may follow a fractional Levy motion which represents a generalization of the FBM. These matters have been reviewed by Molz *et al.* [17]. In any event, it is now widely accepted that the porosities and per-

meabilities of most, if not all, FSPM are scale dependent and fractally distributed and, therefore, contain long-range correlation.

Although well logs, which often provide the data for the porosity and resistivity of FSPM, can have accurate vertical resolution which is important to accurate flow simulation in FSPM, they represent only a small portion of the formations. They are also considered as "point" properties in the sense that they represent the properties of zones of rock that are very small compared with the linear size of FSPM or even the size of the grid blocks that are used in the simulation of flow and transport in FSPM. Seismic data, on the other hand, are areally dense, but vertically sparse, and, therefore, are complementary to well-log data. Such data represent, however, interval-average or "block" properties of rock. Thus, there is a *volume support difference* between the two types of data. If one uses averaged log data, instead of point data, then the difference between their volume support and that of seismic data is reduced to the level that the two sets of data can be integrated with good accuracy in order to produce a more accurate representation of FSPM. Thus, analyzing seismic wave velocities and the associated elastic moduli and bulk density data of FSPM and investigating whether they are scale dependent are also important for the development of more accurate models of FSPM.

The purpose of this paper is to report the results of fractal analysis of measured data for seismic wave velocities and bulk densities of nine FSPM, of which eight are off shore and one is on shore, and to discuss the implications of the results for several important problems in geophysics and rock mechanics. Painter *et al.* [16] previously carried out a fractal analysis of the seismic reflection and amplitudes of some FSPM and argued that these properties may follow a fractional Levy motion (see, however, Ref. [17]).

The plan of this paper is as follows. In the next section we briefly describe the data. Section III presents the methods of analysis that we have utilized in this paper. The results are presented and discussed in Sec. IV, while their implications are considered in Sec. V.

II. DATA

We have analyzed the data for compressional and shear wave velocities—V_p and V_s, respectively—and the bulk density ρ of eight off-shore and one on-shore formations. The off-shore data can be downloaded from an internet site [18], while those for the on-shore porous formation—the South Ellwood field in the Los Angeles basin—were kindly provided to us by Venco, Inc. All the data were in the form of depth-dependence properties and were inferred from the seismic response at roughly equally distanced points about 15 cm apart. Table I summarizes the most important features of the data sets that we have analyzed. Figure 1 presents typical data for well 395A (see Table I) of the mid Atlantic Ridge field, an off-shore field. For comparison, we show in Fig. 2 the same data for well 3247 of the South Ellwood field, the on-shore porous formation.

TABLE I. The porous formations and their locations and the thicknesses of the zones in which the data were collected. n is the number of data points in each set.

Well	Location	Thickness (m)	n
395A	Central Equatorial North Atlantic	155	1376
889B	Iberian Abyssal Plain	40	258
907A	Iceland Plateau	74	486
1137A	Kerguelen Plateau	95	621
1168A	Tasmanian Sea	130	856
1170D	Tasmanian Sea	120	788
1172D	Tasmanian Sea	94	617
1224F	Hawaii-2 Observatory	119	781
1238A	Equatorial Southeast Pacific	408	2088
1241B	Equatorial Northeast Pacific	212	1379
3242	South Ellwood Field	108	710
3247	South Ellwood Field	112	735
3252	South Ellwood Field	103	676

III. ANALYSIS OF THE DATA

Any method that one uses for analyzing the data for FSPM must have two properties. (1) It must yield accurate results even when the number of data points is relatively small (as is often the case with FSPM), and (2) efficient computations using the method must be possible. With these in mind, two methods were used to analyze the data which were shown previously [19] to possess the above two properties. One was the maximum-entropy (ME) method. In this method the spectral density $S(\omega)$ is given by

$$S(\omega) \simeq \frac{a_0}{\left|1 + \sum_{k=1}^{M} a_k z^k\right|^2}, \tag{5}$$

where the coefficients a_k are calculated such that Eq. (5) matches the Laurent series, $S(\omega)=\sum_{-M}^{M} b_i z^i$, with z being the frequency in the z-transform plane, $z \equiv \exp(2\pi i \omega \Delta)$, and Δ the sampling interval in real space. In practice, one first computes [19] the correlation functions

$$C_j = \langle p_i p_{i+j} \rangle \simeq \frac{1}{n-j} \sum_{i=1}^{n-j} p_i p_{i+j}, \tag{6}$$

where n is the number of data points and p_i is the measurement at point i. The coefficients a_i are then calculated from

$$\sum_{j=1}^{M} a_j C_{|j-k|} = C_k, \quad k = 1,2,\ldots,M. \tag{7}$$

As a check of the accuracy of our ME analysis, we also analyzed the data using the wavelet decomposition method [20], by which one calculates the *wavelet-detail coefficients*, or the wavelet transformation, of the measured property $p(r)$, defined by

$$D_j(k) = 2^{-j/2} \int_{-\infty}^{\infty} p(r)\, \psi(2^{-j} r - k)\, dr. \tag{8}$$

Here, ψ is the wavelet function, $k=1,2,\ldots,n$, and the j's are integers. One fixes j and varies k to calculate $D_j(k)$. For each

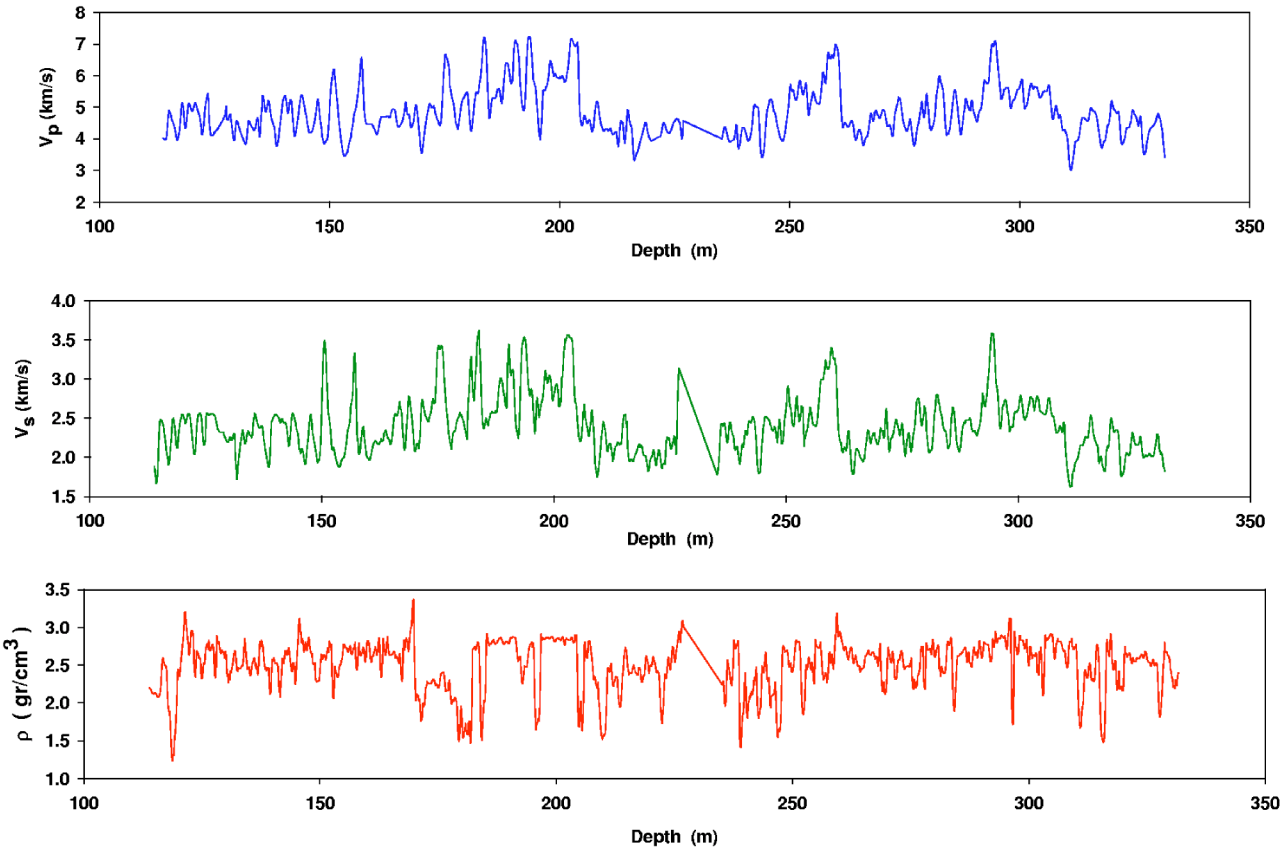

FIG. 1. The data for well 395A in the mid Atlantic Ridge field, an off-shore field.

j one determines n such numbers and calculates their variance $\sigma^2(j)$. Then, it can be shown that [20], regardless of the wavelet ψ, one has

$$\log_2[\sigma^2(j)] = (2H+1)j + \text{const}. \tag{9}$$

Our analysis using the two methods yielded essentially identical results for the Hurst exponent H, hence confirming the accuracy of the results presented below.

IV. RESULTS AND DISCUSSION

In what follows we first describe and discuss the results for the bulk density and wave velocities, after which the results for the elastic moduli are presented.

A. Bulk density and seismic wave velocities

In Fig. 3 we show an example of the spectral density of the data for the compressional wave velocities V_p along well 889B, in the off-shore field in northeast Atlantic Ocean. Over the entire frequency range, the spectral density follows Eq. (4). Figure 4 presents the results for well 3252 in the South Ellwood field, an on-shore field (see Table I). In this case, the spectral density appears to deviate from Eq. (4) at large frequencies, which correspond to small length scales at which the measurement instruments may not have high enough resolution. Similar results were obtained for all the V_p data that we analyzed.

Figure 5 shows the spectral density of the data for the shear wave velocity V_s along well 1137A in the Antarctic, an off-shore field. Once again, over much of the frequency range the data appear to follow a FBM. To compare the results shown in Fig. 5 with those for an on-shore field, we show in Fig. 6 the results for well 3252 of the South Ellwood field. In this case, the spectral density follows Eq. (4) over the entire range of the frequency, hence indicating that the data follow a FBM. Similar results were obtained for all the V_s data that we analyzed.

A typical spectral density for the bulk densities of an off-shore formation is shown in Fig. 7 which presents the results for well 1172D of the Tasmanian Sea field. Although there are some fluctuations in the spectral density, overall $S(\omega)$ follows Eq. (4). For comparison with the data for an on-shore field, we present in Fig. 8 the spectral density for the bulk densties measured along well 3242 of the South Ellwood field.

Our analysis indicates that in all the cases the distributions of the wave velocities and the bulk densities follow the statistics of the FBM and that the Hurst exponents that are estimated by the maximum entropy method and wavelet decomposition technique are completely consistent with each other. Table II presents the estimated Hurst exponents for all the data analyzed.

The numerical errors for fitting Eq. (4) to the computed spectral densities are very small, as the figures also indicate. The possible errors in estimating the Hurst exponents, *due to the uncertainties in the data*, are as follows. According to the

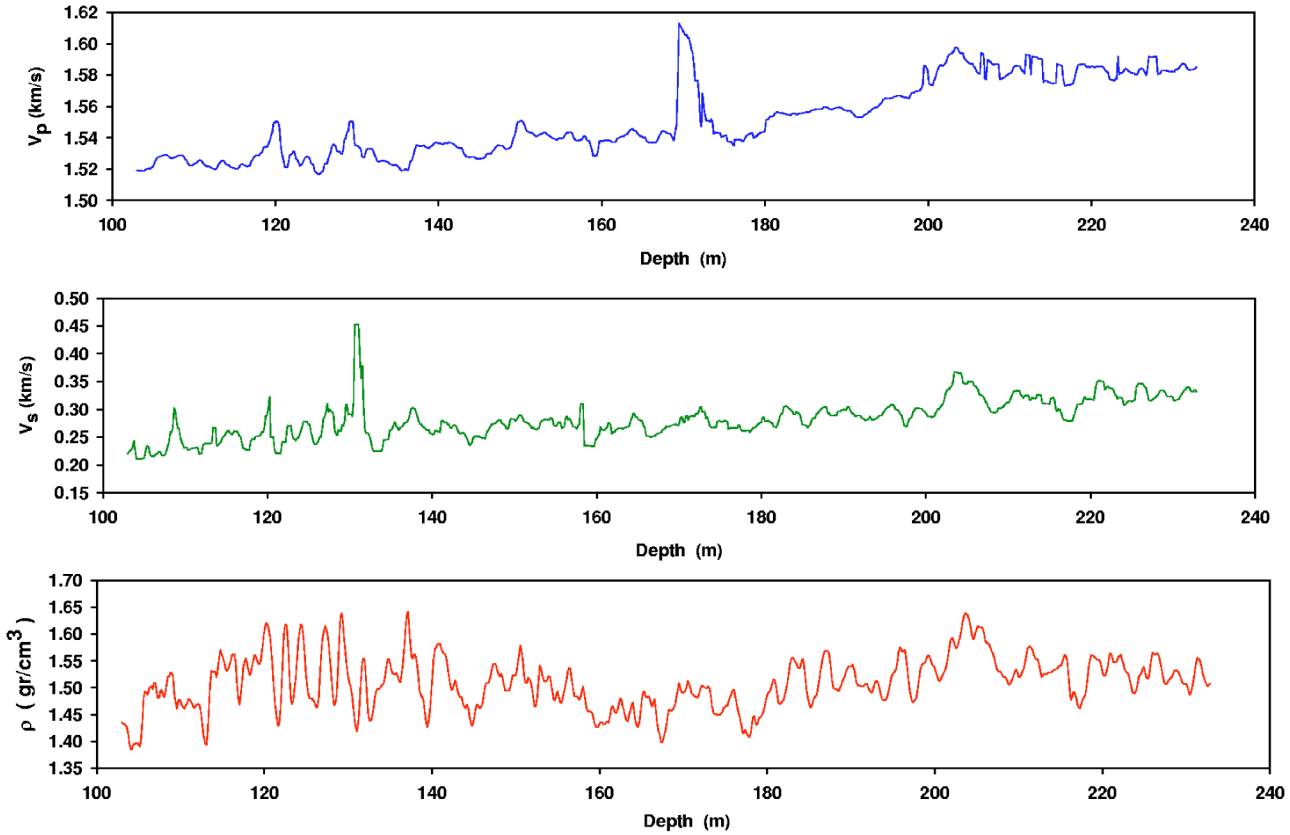

FIG. 2. The data for well 3247A in the South Ellwood field, an on-shore formation.

sources of the data, the estimated errors in the measurement of ρ and V_p are only a few percent, which correspond to very small variations in the estimates of H, about ± 0.03. The same sources also indicate that the estimated errors for V_s are about 10%–15%, which translate into a variation of about ± 0.06 in the estimates of H. Therefore, in all the cases, the maximum possible errors in the estimates of H are well within the range of the variations of H shown in Table II.

Certain features of the results listed in Table II are worth noting. Consider, first, the results for V_p. For the off-shore formations one has $0.29 \leqslant H \leqslant 0.4$, with an average $H \simeq 0.35$. For the Tasmanian Sea formation, the three distributions of V_p are characterized by $0.31 \leqslant H \leqslant 0.4$ which, given the uncertainty in the data, may be approximted by their average 0.35. Similarly, for the on-shore field the Hurst exponent is essentially about 0.40, still to within 13% of the average Hurst exponent of the off-shore formations, hence indicating a possible universal value $H \simeq 0.35 \pm 0.05$.

Consider now the results for the shear wave velocities V_s. The uncertainty in estimating the Hurst exponents for V_s is somewhat larger than that of V_p, with the Hurst exponents for the off-shore formations being more scattered than those

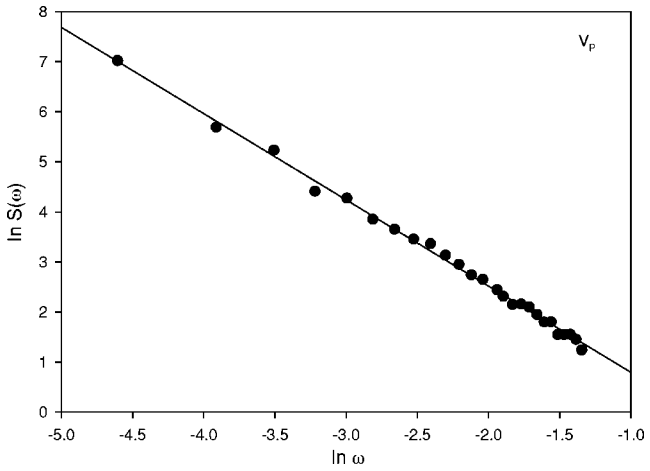

FIG. 3. Spectral density of the comporessional wave velocity V_p along well 889B in northeast Atlantic ocean.

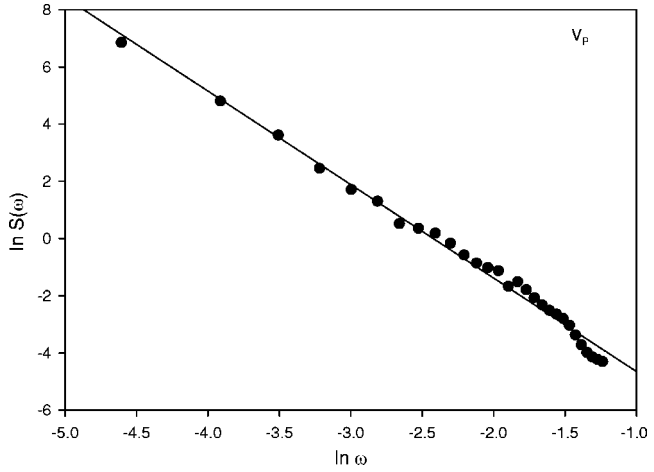

FIG. 4. Same as in Fig. 3, but for well 3252 in the South Ellwood field.

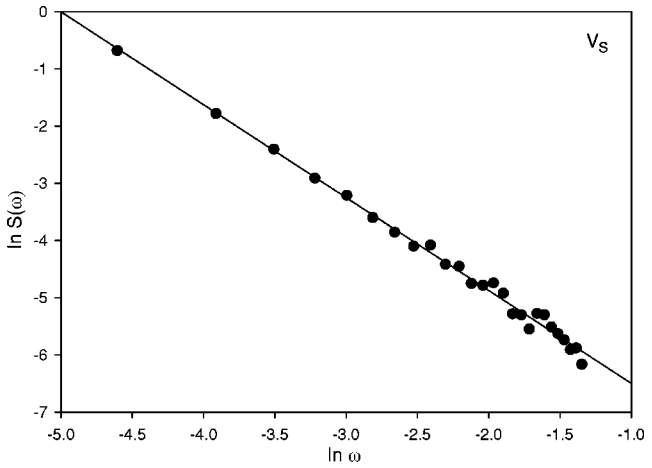

FIG. 5. Spectral density of the shear wave velocity V_s along well 1137A in the off-shore field Antartic.

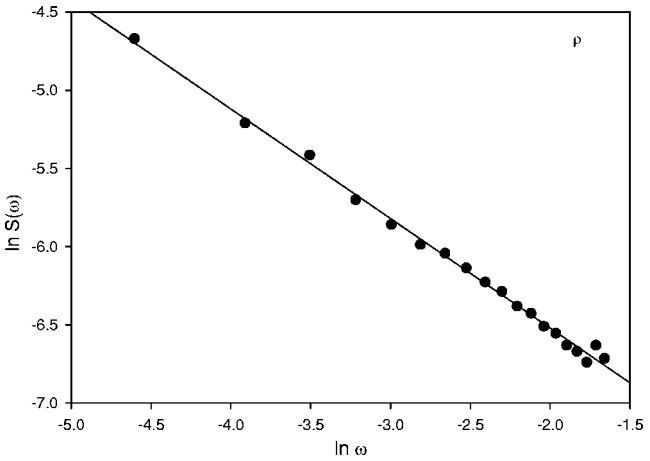

FIG. 7. Spectral density of the bulk density ρ along well 1172D in the Tasmanian Sea field.

of V_p. Roughly half of the formations are characterized by $H<0.5$ with an average value of 0.33, which is close to that of the compressional wave velocities, while the other half are characterized by $0.47 \leqslant H \leqslant 0.60$. The results for the Tasmanian Sea formation are particularly interesting, as the Hurst exponents for V_p and V_s for two of the data sets are practically identical, while they differ significantly for the third set. The difference might be attributed to the differences between the morphology of that zone of the formation in the third set of the data was measured and those of the other two zones or some unknown factor. In the case of the on-shore field, the scatter in the estimated H is large, indicating presumably a very heterogeneous porous formation in which the zones in which the data were collected have very different morphologies.

As for the bulk densities, with one exception (the formation in central equatorial north Atlantic), all the estimates of the Hurst exponent H fall in the range $0.75 \leqslant H \leqslant 1.0$, indicating positive correlations which is what may be intuitively expected. The estimated Hurst exponents for the Tasmanian Sea data are more or less consistent with one another (given the uncertainty in the data), consistent with the pattern for V_p, but different from that of V_s for which two of the estimated Hurst exponents were consistent with one another, but different from the third one. In the case of the on-shore field, the estimated H for the three data sets are clustered around $H \simeq 0.93$.

B. Elastic moduli

Through the classical relations between the wave velocities, the bulk densities, and the elastic moduli, one can estimate the corresponding elastic moduli, given the data for ρ, V_s, and V_p. Consider, for example, the shear modulus G and bulk modulus K. One has

$$G = \rho V_s^2, \tag{10}$$

$$K = \rho V_p^2 - \frac{4}{3} G = \rho \left(V_p^2 - \frac{4}{3} V_s^2 \right). \tag{11}$$

Therefore, given that the wave velocities and the bulk density appear to be fractally distributed, one may also expect the elastic moduli to be scale dependent and fractally distrib-

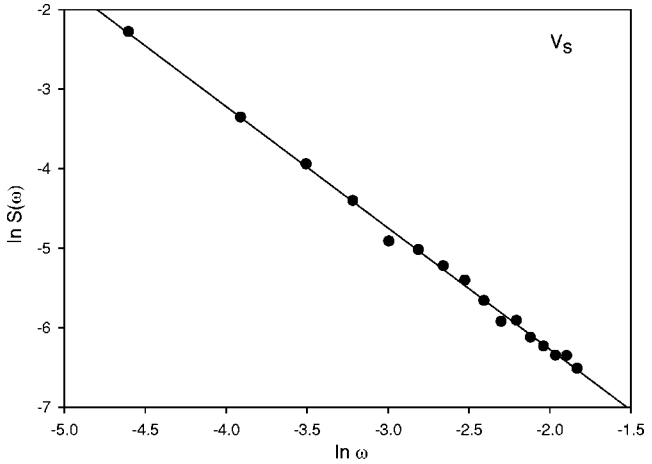

FIG. 6. Same as in Fig. 5, but for well 3252 in the South Ellwood field.

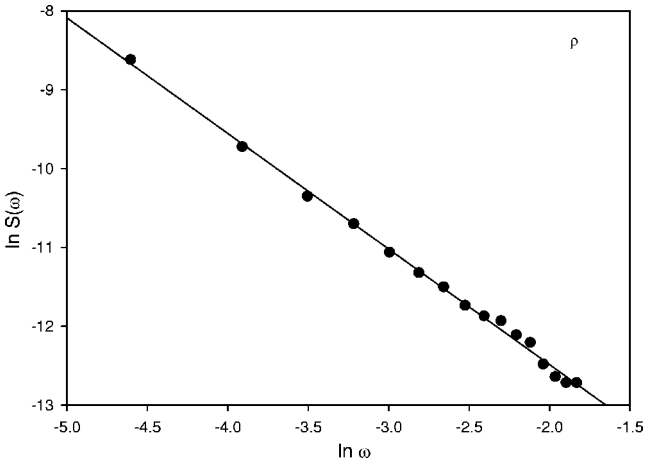

FIG. 8. Same as in Fig. 7, but for well 3242 in the South Ellwood field.

TABLE II. The porous formations and the resulting Hurst exponents for the seismic wave velocities V_p and V_s, the bulk density ρ, the shear modulus G, bulk modulus K, and Young's modulus Y.

Well	Location	H_{V_p}	H_{V_s}	H_ρ	H_G	H_K	H_Y
395A	Central Equatorial North Atlantic	0.39	0.57	0.62	0.49	0.38	0.52
889B	Iberian Abyssal Plain	0.29	0.36	0.85	0.35	0.33	0.31
907A	Iceland Plateau	0.36	0.29	0.70	0.56	0.27	0.38
1137A	Kerguelen Plateau	0.35	0.39	0.93	0.52	0.38	0.35
1168A	Tasmanian Sea	0.40	0.53	0.75	0.60	0.50	0.34
1170D	Tasmanian Sea	0.31	0.32	0.80	0.39	0.34	0.33
1172D	Tasmanian Sea	0.35	0.37	0.87	0.36	0.28	0.28
1224F	Hawaii-2 Observatory	0.38	0.47	0.77	0.45	0.33	0.38
1238A	Equatorial Southeast Pacific	0.37	0.50	0.94	0.49	0.36	0.40
1241B	Equatorial Northeast Pacific	0.33	0.60	1.00	0.64	0.35	0.45
3242	South Ellwood Field	0.41	0.51	0.98	0.51	0.42	0.51
3247	South Ellwood Field	0.43	0.62	0.89	0.56	0.35	0.46
3252	South Ellwood Field	0.36	0.42	0.93	0.47	0.37	0.39

uted with long-range correlations. However, if the data for V_s, V_p, and ρ follow the statistics of a FBM (albeit with different values of the Hurst exponent H), the distributions of G and K (and that of the Young's modulus) do not, in principle, have to be FBM also. To see this, recall the basic definition of a random variable $X(r)$ that follows the statistics of a FBM. One has [21]

$$P\{X(r+h)-X(r)\leqslant x\}=\frac{h^{-H}}{\sqrt{2\pi}}\int_{-\infty}^{x}\exp\left(-\frac{y^2}{2h^{2H}}\right)dy, \tag{12}$$

where P denotes the probability. Therefore, assuming that the random variables $X(r)$ and $Y(r)$ are independent, then the Fourier transform $\hat{f}_\omega(r)$ of the probability distribution $f_z(r)$ of a random variable $Z(r)=X(r)Y(r)^2$ is given by [22,23]

$$\hat{f}_\omega(r)=\langle\exp[i\omega X(r)Y(r)^2]\rangle, \tag{13}$$

where $\langle\cdot\rangle$ denotes expectation value of the quantity. If $X(r)$ and $Y(r)$ denote, respectively, the stochastic variables bulk density ρ and shear wave velocity V_s that are distributed according to a FBM with the Hurst exponents H_ρ and H_{V_s}, Eqs. (12) and (13) imply that the Fourier transform $\hat{f}_\omega(r)$ of the probability distribution function $f_G(r)$ of $G=\rho(r)V_s^2(r)$ is given by

$$\begin{aligned}\hat{f}_\omega(r)&=\frac{r^{-H_\rho-H_{V_s}}}{\sqrt{2\pi}}\int_{-\infty}^{\infty}\int_{-\infty}^{\infty}\exp\left(-\omega xy-\frac{x^2}{2r^{2H_\rho}}-\frac{y^2}{2r^{2H_{V_s}}}\right)dxdy\\&=\frac{r^{-H_{V_s}}}{\sqrt{2\pi}}\int_{-\infty}^{\infty}\exp\left(-\frac{1}{2}r^{2H_\rho}\omega^2y^4-\frac{y^2}{2r^{2H_{V_s}}}\right)dy.\end{aligned} \tag{14}$$

Therefore,

$$f_G(r)=\frac{1}{2\pi r^{H_\rho+H_{V_s}}}\int_{-\infty}^{\infty}\exp\left(-\frac{G^2}{2r^{2H_\rho}y^4}-\frac{y^2}{2r^{2H_{V_s}}}\right)\frac{dy}{y^2}, \tag{15}$$

which, in general, is not identical with what Eq. (12) would yield.

However, we find, surprisingly, that the elastic moduli follow, at least approximately, the statistics of a FBM, albeit with a value of H different from those obtained for ρ, V_p, and V_s. Figure 9 shows, for example, the results for the shear moduli measured along well 1137 in the Antarctic, exhibiting reasonable power-law scaling for the spectral density. Figure 10 presents similar results for well 3252 in South Ellwood field, exhibiting even more accurate power-law scaling of the spectral density of G. We find that for the bulk modulus K, $0.27\leqslant H\leqslant 0.38$, with an average value of about 0.33, whereas for the Young's modulus Y, $0.28\leqslant H\leqslant 0.45$, with an average value of about 0.36, within the range of variations of the Hurst exponent for K. Table II summarizes the results for

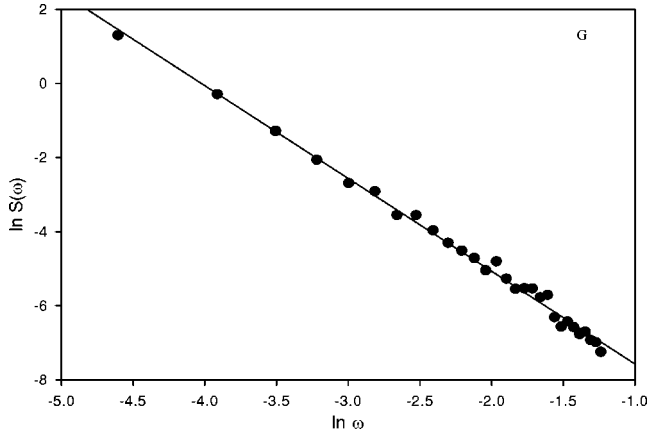

FIG. 9. Spectral density of the shear moduli along well 1137 in the Antartic field.

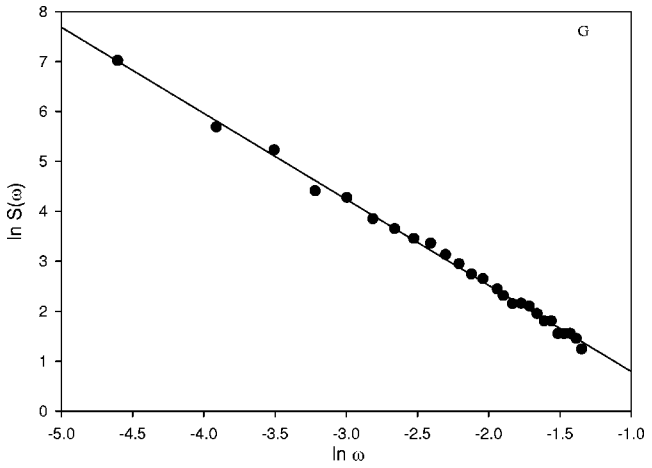

FIG. 10. Same as in Fig. 9, but for well 3252 of the South Ellwood field

all the Hurst exponents of all the elastic moduli. The estimated errors for the Hurst exponents of the elastic moduli should be about the same as those of V_s.

V. IMPLICATIONS OF THE RESULTS

The results presented above have at least three important implications.

(i) The scale dependence of the elastic moduli implies that, in order to carry out numerical simulation of deformation of rock samples and compute its mechanical properties, the computational grid which is used in the numerical simulations must be large and the elastic constants of the grid blocks must be correlated and fractally distributed. The precise way by which a fractal distribution of the local elastic moduli is used in the computational grid representing the rock is important. Several models have already been suggested for simulating fluid flow in rock [1,3] which, by appropriate modifications, can be used for studying rock's mechanical properties. Lu *et al.* [24] suggested, for example, a method for generating a realistic model of heterogeneous rock based on fractal statistics and the distribution of the facies (that is, zones of rock with distinct distributions of local flow and transport properties) in which large-scale facies distributions are generated by a stochastic method and FBM distributions are used for generating the distributions of the local permeabilities within the facies. The same model may be used for studying mechanical properties of rock, with the local permeabilities in the model of Lu *et al.* replaced by the elastic moduli [25].

(ii) Wave propagation in heterogeneous media, such as rock, has been studied for decades (see, for example, Sato and Fehler [26]). The phenomenon is important in view of the fact that the acoustic properties of rock provide clues to its heterogeneous morphology. In particular, the processing of seismic data and the delineation of rock structure from them have been problems of great interest for decades. However, given that, according to our results, the wave velocities, density, and elastic moduli appear to be scale dependent and fractally distributed, one should study the problem of how a wave front propagates in a heterogeneous medium with fractal distributions of the local elastic moduli. We have recently shown [27] that acoustic waves in such media will be *localized in any dimension*; i.e., one can define a localization length L_ℓ such that for distances $L > L_\ell$ from the wave source the wave amplitude will be too small to be detected. This result has important implications for interpreting seismic records in terms of the solution of the classical acoustic wave equation in which no correlation of the type discovered by our analysis is included. In particular, if a heterogeneous rock of linear dimension L, with the type of heterogeneities discovered in this paper, is to be surveyed by a seismic method, the seismic records will not provide any useful information on the rock morphology for length scales $L > L_\ell$.

In addition, we have shown [28] that, unlike homogeneous media or those with uncorrelated heterogeneities in the elastic constants, the shape of a wave front in media with scale-dependent elastic constants is very rough (whereas in homogeneous or weakly heterogeneous media the front is smooth), with its roughness structure related closely to the Hurst exponent H for the distribution of the local elastic constants. More precisely, if we define the width $w(L,t)$ of the wave front by

$$w(L,t) = \langle [h(x,t) - \langle h \rangle_L]^2 \rangle^{1/2}, \tag{16}$$

where $h(x,t)$ is the height of the wave front (with respect to a reference plane) at position x at time t and $\langle h \rangle_L$ is its average over a horizontal segment of L, then according to the dynamic scaling theory of Family and Vicsek [29] one has

$$h(x,t) - \langle h \rangle_L \sim t^{\beta} f(x/t^{\beta/\alpha}), \tag{17}$$

where α and β are two exponents and $f(u)$ is a scaling function. In particular,

$$w(L,t) \sim L^{\alpha} g(t/L^{\beta/\alpha}), \tag{18}$$

with α being the roughness exponent of the wave front. We find that [28] if the local elastic moduli of a heterogeneous medium, such as rock, are distributed according to a FBM with a Hurst exponent H, then $\alpha = H$, an important result, in our view, that connects the static morphology of a porous formation (characterized by the Hurst exponent H) to its dynamical properties (w and α).

(iii) Over the past several decades, many models have been proposed to study how cracks propagate in heterogeneous rock. However, fracture propagation in rock, or any heterogeneous material for that matter, depends sensitively on the distribution of its local elastic constants [30] and, in particular, the correlations between them. At the same time, in practically all the previous models of fracture propagation in rock, the correlations of the type described in this paper were not considered. Our preliminary simulations indicate that inclusion of a scale-dependent elastic constant gives rise to complex fracture patterns in rock, which better resemble the observed natural fracture patterns in rock [1,3].

We emphasize that although the data that we have analyzed appear to be well represented by the FBM, it may be that a more precise analysis with more extensive (and possibly more accurate) data reveals that the data follow more general fractal distributions. In our view, however, the most important aspect of the work is *not* the precise analytical form of the fractal distribution (such as the FBM) that the data may follow, but the discovery of the long-range correlation in the data that the analysis indicates to exist and its implications for the important problems in geophysics and rock mechanics that we discussed above.

ACKNOWLEDGMENTS

The authors are grateful to the management of the companies that provided them with their data. They would like to thank Barry D. Hughes for his expert help in the analytical analysis of the relationship between the probability distribution functions of the elastic moduli and those of the wave velocities and the bulk density, as well as Alireza Bahraminasab, M. Reza Rahimi Tabar, and S. Mehdi Vaez Allaei for many useful discussions. The work of the second author was supported by the NIOC.

[1] P. M. Adler, *Porous Media: Geometry and Transports* (Butterworth-Heinemann, Stoneham, MA, 1992); P. M. Adler and J.-F. Thovert, *Fractures and Fracture Networks* (Kluwer, Dordrecht, 1999).
[2] S. Torquato, *Random Heterogeneous Materials* (Springer, New York, 2002).
[3] M. Sahimi, Rev. Mod. Phys. **65**, 1393 (1993); *Flow and Transport in Porous Media and Fractured Rock* (VCH, Weinheim, Germany, 1995).
[4] T. A. Hewett, in *Proceedings of the Society of Petroleum Engineers Annual Meeting*, New Orleans, 1986 (Society of Petroleum Engineers, Richardson, TX, 1986), SPE Paper 15386.
[5] J. Bruining, D. van Batenburg, L. W. Lake, and P. A. Yang, Math. Geol. **29**, 823 (1997).
[6] S. E. Crane and K. M. Tubman, in *Proceedings of the Society of Petroleum Engineers Annual Conference* (Society of Petroleum Engineers, Richardson, TX, 1990), SPE Paper 20606.
[7] M. Sahimi and Y. Yortsos, in *Proceedings of the Society of Petroleum Engineers Annual Conference* (Society of Petroleum Engineers, Richardson, TX, 1990), SPE Paper 20476.
[8] I. J. Taggart and H. A. Salisch, APEA J. **31**, 377 (1991).
[9] Y. Aasum, M. G. Kelkar, and S. P. Gupta, SPE Form. Eval. **6**, 11 (1991); P. Grindrod and M. D. Impey, Water Resour. Res. **29**, 4077 (1993).
[10] H. H. Hardy, in *Proceedings of the Society of Petroleum Engineers Annual Conference* (Society of Petroleum Engineers, Richardson, TX, 1990), SPE Paper 20476.
[11] M. Sahimi, H. Rassamdana, and A. R. Mehrabi, in *Fractal Aspects of Materials*, edited by Fereydoon Family, B. Sapoval, P. Meakin, and R. Wool, Mater. Res. Soc. Symp. Proc. No. 367 (Materials Research Society, Pittsburgh, 1995), p. 203.
[12] G. J. Goggin, M. A. Chandler, G. Kocurek, and L. W. Lake, SPE Form. Eval. **7**, 7 (1992).
[13] F. J. Molz and G. K. Boman, Water Resour. Res. **29**, 3769 (1993).
[14] A. J. Desbarats and S. Bachu, Water Resour. Res. **30**, 673 (1994).
[15] S. P. Neuman, Geophys. Res. Lett. **21**, 349 (1994).
[16] S. Painter, Math. Geol. **27**, 813 (1995); S. Painter, G. Beresford, and L. Paterson, Geophysics **60**, 1187 (1995).
[17] F. J. Molz, H. Rajaram, and S. Lu, Rev. Geophys. **42**, RG1002 (2004).
[18] See http://www.ldeo.columbia.edu/BRG/ODP/DATABASE/DATA/search.html
[19] A. R. Mehrabi, H. Rassamdana, and M. Sahimi, Phys. Rev. E **56**, 712 (1997).
[20] P. Flandrin, IEEE Trans. Inf. Theory **38**, 910 (1992).
[21] G. Samorodnitsky and M. S. Taquu, *Stable Non-Gaussian Random Process* (Chapman and Hall, New York, 1994); P. Embrechts and M. Maejima, *Self-Similar Process* (Princeton University Press, Princeton, 2002).
[22] A. Papoulis, *Probability, Random Variables, and Stochastic Process* (McGraw-Hill, New York, 1965).
[23] B. D. Hughes, *Random Walks and Random Environments* (Oxford University Press, London, 1995), Vol. 1.
[24] S. Lu, F. J. Molz, G. E. Fogg, and J. W. Castle, Hydrogeol. J. **10**, 475 (2002).
[25] S. M. Vaez Allaei and M. Sahimi (unpublished).
[26] H. Sato and M. Fehler, *Seismic Wave Propagation and Scattering in the Heterogeneous Earth* (Springer, New York, 1998).
[27] F. Shahbazi, A. Bahraminasab, S. M. Vaez Allaei, M. Sahimi, and M. R. Rahimi Tabar (unpublished).
[28] S. M. Vaez Allaei and M. Sahimi (unpublished).
[29] F. Family and T. Vicsek, J. Phys. A **18**, L75 (1985).
[30] M. Sahimi, *Heterogeneous Materials* (Springer, New York, 2003), Vol. II.